Estuaries and Coasts (2020) 43:943–959
https://doi.org/10.1007/s12237-019-00690-3

SPECIAL ISSUE: IMPACT OF 2017 HURRICANES

A System Level Analysis of Coastal Ecosystem Responses to Hurricane Impacts

C. J. Patrick[1] · L. Yeager[2] · A. R. Armitage[3] · F. Carvallo[1] · V. M. Congdon[2] · K. H. Dunton[2] · M. Fisher[4] · A. K. Hardison[2] · J. D. Hogan[1] · J. Hosen[5] · X. Hu[1] · B. Kiel Reese[1] · S. Kinard[1] · J. S. Kominoski[6] · X. Lin[2,7] · Z. Liu[2] · P. A. Montagna[1] · S. C. Pennings[8] · L. Walker[1] · C. A. Weaver[1] · M. Wetz[1]

Received: 16 January 2019 / Revised: 18 November 2019 / Accepted: 17 December 2019 / Published online: 26 April 2020

Abstract

Tropical cyclones are major disturbances for coastal systems. Hurricane Harvey made landfall in Texas, USA, on August 25, 2017 as a category 4 storm. There were two distinct disturbances associated with this storm that were spatially decoupled: (1) high winds causing direct damage and storm surge, and (2) high rains causing scouring floods and significant discharge of fresh water carrying carbon and nutrients to estuaries. Here, we provide a synthesis of the effects of Hurricane Harvey on biogeochemical, hydrographic, and biotic components of freshwater and estuarine systems and their comparative resistance and resilience to wind- and rain-driven disturbances. Wind-driven disturbances were most severe along the coastal barrier islands and lower estuaries, damaging mangroves and seagrass and increasing sediment coarseness. Rain-driven disturbances were most pronounced within freshwater streams and the upper estuaries. Large volumes of freshwater run-off reduced the abundance of riverine fauna and caused hypoxic and hyposaline conditions in the estuaries for over a week. In response to this freshwater input event, benthic fauna diversity and abundance decreased, but mobile fauna such as estuarine fishes did not markedly change. Although hydrographic and biogeochemical components were highly perturbed, they returned to baseline conditions within days. In contrast, biotic components demonstrated lower magnitude changes, but some of these organisms, particularly the sedentary flora and fauna, required weeks to months to return to pre-storm conditions, and some did not recover within the 6 months reported here. Our synthesis illustrates that resistance and resilience of system components may negatively co-vary and that structural components of coastal systems may be the most vulnerable to long-term changes following tropical cyclones.

Keywords Disturbance · Coastal ecosystem · Fish · Invertebrates · Biogeochemistry · Mangroves · Seagrass · Hurricane Harvey

Communicated by Steven Litvin

Electronic supplementary material The online version of this article (https://doi.org/10.1007/s12237-019-00690-3) contains supplementary material, which is available to authorized users.

✉ C. J. Patrick
christopher.patrick@tamucc.edu

[1] Texas A&M University-Corpus Christi, 6300 Ocean Dr, Corpus Christi, TX 78412, USA

[2] University of Texas Marine Science Institute, 750 Channel View Dr, Port Aransas, TX 78373, USA

[3] Texas A&M University at Galveston, 200 Seawolf Pkwy, Galveston, TX 77554, USA

[4] Texas Parks and Wildlife Department, 346 Oaks Trail #100, Garland, TX 75043, USA

[5] Yale University, New Haven, CT 06520, USA

[6] Department of Biological Sciences, Florida International University, Miami, FL 33199, USA

[7] East China Normal University, Shanghai, China

[8] Department of Biology and Biochemistry, University of Houston, Houston, TX 77204, USA

Introduction

Hurricanes and tropical cyclones are one of the most destructive natural disturbances to coastal environments, causing severe disruptions via storm surge, saltwater intrusion, wind damage, and flooding (Paerl et al. 2001). Storm surges inundate terrestrial and freshwater habitats with salt water, and associated waves scour estuarine benthic habitats (Mallin et al. 1999). High winds cause widespread damage to both natural and built environments, creating significant fluxes of organic material and changing vegetation structure (Adger et al. 2005; Armentano et al. 1995; Laurance and Curran 2008). Extreme precipitation mobilizes entrained sediments and nutrients and causes scouring floods in riverine ecosystems (Avery et al. 2004; Schaefer et al. 2000).

Global climate models predict that the severity of these events will increase, and the spatial distribution of regions that regularly experience hurricanes will shift poleward over the next century (IPCC 2018; Knutson et al. 2010; Mann and Emanuel 2006). This makes it imperative to understand the factors that dictate how whole ecosystems respond to hurricanes. However, the opportunistic nature of the majority of ecological studies of storm impacts has resulted in a body of literature dominated by studies focused on particular components of study systems and often lacking adequate controls in space and time (Pruitt et al. 2019). Although there are decades of studies documenting the effects of tropical cyclones on both developed and natural systems, a conceptual understanding of factors that dictate ecosystems response to a given storm is lacking (Pruitt et al. 2019).

A key concept in understanding how ecosystems respond to extreme events is ecosystem stability, which we consider separately as ecosystem resistance and resilience. We use the following classic definitions: *resistance* is a measure of the system's ability to remain essentially unchanged in the face of a perturbation, while *resilience* is a measure of a system's ability to return to pre-perturbation condition (Harrison 1979; Pimm 1984). The resistance-resilience framework can be used to enhance our understanding of the vulnerability of socio-ecological coastal systems to extreme stress events (Adger et al. 2005). Taking a system level viewpoint, by quantifying and comparing the resistance and resilience of different components of coastal ecosystems, we can determine where the greatest vulnerabilities lie and what intrinsic and extrinsic factors are responsible for that vulnerability. Ultimately, this type of analysis is a step toward improving understanding and enhancing predictive power about the impacts of future storms and, ultimately, may help identify steps that can be taken to reduce impacts or to plan for their effects.

Barring a concerted research consortium approach to studying future storms (Pruitt et al. 2019), meta-analysis offers us a path toward synthetic understanding of the mechanisms controlling ecosystem responses to tropical cyclones. Two complimentary approaches to meta-analysis can be employed: (1) a broad survey of ecosystem responses across multiple storms through space and time or (2) an in-depth comparative analysis of ecosystem responses to a single event. The former approach has the advantage of potentially yielding broad generalizations, such as the observation that forest fragmentation synergistically enhances the destructive effects of wind disturbance on tropical forests (Laurance and Curran 2008). However, in-depth comparative analysis of a single event can provide understanding about cascading interactions driving responses. For example, Paerl et al. (2001) documented that high nitrogen loads following Hurricanes Dennis, Floyd, and Irene into the Pamlico Sound, NC, combined with long water residence time to drive a cascade of impacts including sustained bottom water hypoxia, increased algal biomass and increased in the instances of fish disease. There are few examples of such synthetic studies of ecosystem responses to tropical cyclones (Armentano et al. 1995; Greening et al. 2006; Paerl et al. 2001; Xi 2015) and fewer still that contain quantitative analysis among ecosystems rather than verbal comparisons through literature review. Basic questions that remain unanswered include the following: How does resistance and resilience to tropical cyclones vary among ecosystem types (estuaries, barrier islands, and coastal rivers) and components (hydrographic, biogeochemical, mobile fauna, etc.) within ecosystems? What role does the identity of the stressor (wind force, rainfall, storm surge) play in mediating these patterns?

In the fall of 2017, the Atlantic and Caribbean islands experienced one of the most devastating hurricane seasons in recorded history, with three major storms including Irma, Maria, and Harvey. Here we use one of these storms, Hurricane Harvey, as a case study. We leveraged the high density of research programs evaluating the impacts of the event to document patterns of resistance and resilience among different coastal habitats (estuaries, barrier islands, coastal plain streams, and rivers) in response to different stressors. We include both a synthetic analysis of the pattern of resistance and resilience within and among ecosystems and ecosystem components and a series of analyses exploring individual responses to the disturbance event.

In addition to being one of the few such analyses of its kind, the present study has several novel features that add to our understanding of tropical cyclone affects. First, our dataset covers several different embayments and watersheds allowing for comparison among systems that experienced different levels of wind, rain, and storm surge stress. Hurricanes have a wetter side and stronger side where the storm picks up moisture and speed over warm water and then loses that energy as it rotates over land. Our region includes both the wet and dry sides of the storm, as well as the area affected by the high rotational speeds of the eye of the storm. Second, we are not aware of any similar quantitative syntheses in sub-tropical coastal regions. Third, we employ the resistance-resilience conceptual framework an approach to quantify and comparing

ecosystem responses, an approach that has not been used in other syntheses. The goal of these analyses is to provide a broad, ecosystem-level view of Hurricane Harvey's impacts on the affected coastal ecosystems.

Methods

Study System

The study focused on the south Texas coast, a sub-tropical area at the transition between the mesic Coastal Plain and arid Sonoran Floristic Province (Noss et al. 2015; Sorrie and Weakley 2001). The region consists of a series of lagoonal estuaries protected by barrier islands and connected to the Gulf of Mexico by several narrow inlets (Montagna and Li 2010). Oriented from southwest to northeast, hurricane force winds impacted multiple estuaries, including the upper Laguna Madre behind Padre Island, Corpus Christi Bay behind Mustang Island, the Mission-Aransas Bay complex behind San Jose Island, and San Antonio Bay behind Matagorda Island (Fig. 1). These estuaries are home to productive fish and shellfish fisheries valued by commercial fisherman ($196 million USD commercial catch value) and recreational anglers (NOAA 2018).

At the point where Hurricane Harvey made landfall, strong winds (Category 4, gusts up to 241 km h^{-1}) were recorded on Mustang and San Jose Islands and within the Mission-Aransas estuarine system (Fig. 1). High speed winds extended further east than west, with areas 40 km to the east experiencing 190kmph winds and areas 40 km to the west experiencing 144kmph winds (Fig. 1). In the area northeast of the eye, storm surge raised water levels 2–3 m above sea level within Copano, Aransas, San Antonio, and Matagorda Bays. Harvey lingered over Victoria, Texas for 2 days, and rainfall totals of 44 cm were recorded in Victoria County just 86 km from the landfall zone, whereas 65 km to the southwest in Nueces County (which includes the city of Corpus Christi), rainfall totals were only 9 cm (Source: National Weather Service). Thus, the effects of wind and rain disturbances were decoupled spatially with different bays experiencing different combinations of wind and precipitation intensity.

Hurricane impact data were synthesized from freshwater, estuarine, and coastal wetland systems across the Texas coast ranging from the Upper Laguna Madre to San Antonio Bay (Fig. 1). Systems include nine coastal rivers, two barrier islands, and four major estuary complexes. Samples consist of synoptic grab samples for water chemistry and nutrients, high-frequency data collections, physical habitat measurements, and quantitative surveys for flora and fauna. There

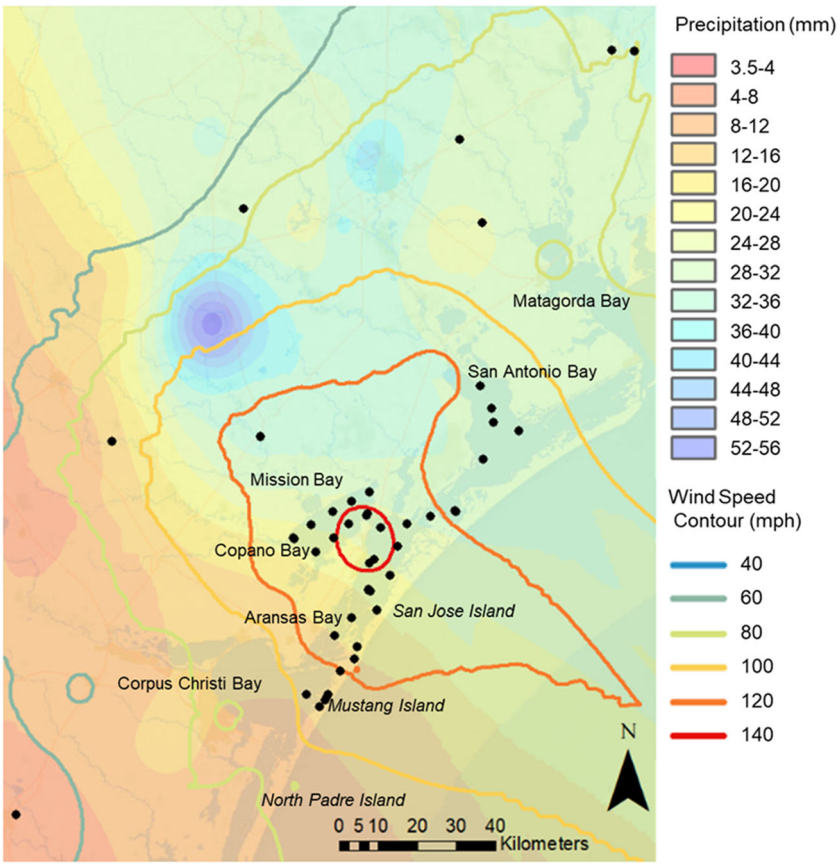

Fig. 1 Spatial distribution of hurricane weather and sampling sites. Total precipitation from August 25 to 30 was interpolated using an inverse spline from weather stations throughout the region and is displayed as a color map (source: National Weather Service). Maximum wind speed during the storm was similarly interpolated from weather stations and displayed as contours with red indicating the zone of highest wind speeds. Sampling stations from which data were collected are depicted as black dots

were 51 unique stations with temporal sampling of multiple responses in fixed positions in the dataset (Fig. 1), as well as repeated monthly sampling in random locations within estuaries for mobile fauna ($n = 20$ replicates per month per gear type). A complete list of station locations and parameters measured is found in S1 Supplementary Material.

Storm Data

Wind speed data in the form of maximum 10 m wind gust during the storm and precipitation totals around the August 26th landfall date from August 24 to August 30, 2017 were provided by National Weather Service Offices in Corpus Christi, Brownsville, Austin/San Antonio, and Houston/Galveston, TX. River discharge data were downloaded from USGS gauging stations co-located with study sites within the affected region (USGS 2016).

Hydrography

Continuous Water Quality Sampling At one station in San Antonio Bay, Hydrolab DS5X sondes (OTT HydroMet, Loveland, CO, USA) were deployed on the surface and bottom for continuous measurement (at 15-min intervals) of salinity, temperature, and dissolved oxygen from May to December of 2017. MiniDOT dissolved oxygen and temperature loggers (PME, Vista, CA, USA) were deployed in nine rivers from mid-August to December of 2017. Data for the entire monitoring period are reported as 24-h averages of the high-frequency (15-min interval) data. At two stations in Copano Bay, salinity, temperature (°C), and turbidity (NTU) were measured continuously every 15 min by YSI 6600 V2 sondes mounted on sampling platforms 0.5 m above the seafloor as part of the Mission-Aransas National Estuarine Research Reserve (MANERR) system wide monitoring program. Data are available for download at the Centralized Data Management Office (CDMO, http://cdmo.baruch.sc.edu). Sondes in San Antonio Bay were calibrated prior to deployment and traded out on timescales from 5 days to 2 weeks depending on biofouling and weather conditions. Sondes in the coastal rivers were cleaned, and data were downloaded at 2–4-week intervals. Sondes underwent rigorous post-deployment quality control check upon retrieval to ensure data were not affected by biofouling or faulty probes.

Synoptic Water Quality Sampling Coastal rivers were visited every 2 to 4 weeks from August to December 2017. During each visit, water quality measurements were taken at four stations within a fixed 75-m reach of stream using a YSI ProDSS Multiparameter Probe to collect turbidity (NTU), dissolved oxygen (mg L^{-1}), temperature (°C), conductivity (μs cm^{-1}), and pH. Probes were calibrated prior to use. Water quality measurements were taken at four stations in San Antonio Bay that were visited at 2-week intervals from March to December 2017 to collect dissolved oxygen (mg L^{-1}), temperature (°C), salinity, and pH. Secchi disk measurements were taken concurrently with water quality sampling in San Antonio Bay.

Biogeochemistry

Water samples in the rivers were collected in replicates of four every 2 to 4 weeks from August to December 2017. Samples were filtered in the field using 0.2-μm filters and frozen until analysis for DOC (dissolved organic carbon), NO_3^-, NH_4^+, and orthophosphate. Samples were analyzed for DOC as non-purgeable organic carbon (NPOC) using a Shimadzu TOC-vcph with attached TNM-1 nitrogen analyzer (Shimadzu Corporation; Kyoto, Japan). Samples were first acidified with 2% 2 N HCl and sparged with zero CO_2 air for 6 min to remove inorganic carbon, then they were analyzed for nutrients using a Lachat Flow Injection Auto-analyzer for NO_3^-, NH_4^+, and orthophosphate. Estuarine surface water samples were collected by the MANERR for monthly nutrient concentrations at two stations in Copano Bay. Concentrations of NO_3^-, NO_2^-, NH_4^+, and PO_4^{3-} were determined on a nutrient autoanalyzer using standard colorimetric methods.

For water carbonate chemistry quantification, surface water samples were collected using a Van Dorn sampler at five system wide water quality monitoring program (SWMP) stations in the Mission-Aransas Estuary on a biweekly or monthly basis in 2017 and at seven stations in San Antonio Bay on a quarterly basis prior to June 2017 and then on a biweekly to monthly basis from June to December 2017. Total dissolved inorganic carbon (DIC) and pH were analyzed on these samples. Methods on sample collection, preservation, and analysis can be found in Yao and Hu (2017). Surface water CO_2 partial pressure (pCO_2) at in situ temperature was calculated using lab measured DIC and pH (at 25 °C) as the input variables. The carbonic acid dissociation constants were from Millero (2010), dissociation constant of bisulfate was from Dickson et al. (1990), and borate concentration was from Uppstrom (1974).

Wind speed data used in these two estuaries were downloaded from the NOAA meteorological stations located at Seadrift (Station 8,773,037, for San Antonio Bay) and Port Aransas (Station 8,775,237, for Mission-Aransas Estuary). As the anemometers are deployed at heights lower than 10 m (7.6 and 9.0 m, respectively), wind speed at 10 m was calculated using the power function in Hsu et al. (1994). Mole fraction atmospheric CO_2 in dry air (xCO_2) was downloaded from http://www.esrl.noaa.gov/gmd/ccgg/trends. Atmospheric pCO_2 was then calculated using xCO_2, salinity, and temperature (Weiss and Price 1980). CO_2 flux was calculated using the following equation:

$$F = kK_0(\mathrm{pCO_2, water} - \mathrm{pCO_2, air})$$

where k (m day^{-1}) is the gas transfer velocity calculated from wind speed. We used the formulation in Jiang et al. (2008); K_0 (mol m^{-3} atm^{-1}) is the gas solubility at in situ temperature and salinity (Weiss 1974). A positive F value indicates CO_2 degassing to the atmosphere.

For estuarine chloropigment and accessory pigment measurements, surface water samples (1 L) were collected ~ 0.1 m below the surface and stored on ice until filtration through precombusted GF/F filters (Whatman 47 mm 0.7 μm). Pigments from GF/F filters and thawed sediments were extracted twice using acetone according to the protocol of Sun et al. (1991). Briefly, 3–6 mL of acetone were added to the samples in centrifuge tubes, sonicated for 15 min, and centrifuged for 10 min. The supernatant was further filtered through a 0.2-μm syringe Nylon filter. This extraction procedure was repeated again, and the filtered supernatants were combined. The pigment analysis was accomplished through high performance liquid chromatography (HPLC) with UV absorbance detection according to McTigue et al. (2015). The mobile phases included 28 mM tetrabutylammonium acetate in methanol (30%: 70%; eluent A) and methanol (eluent B). After eluting through a C8 column (Agilent Eclipse XDB, 3.5 μm, 4.6 mm diameter × 150 mm length), individual pigments were detected by UV–Vis absorbance at a wavelength of 450 nm. Quantification was based on authentic standards (DHI and Sigma-Aldrich). The relative amounts of diatom and cyanobacteria were calculated based on established algorithms from the accessory pigments (Reyna et al. 2017).

Mobile Biota

Gill nets were set during a 10-week period each fall, beginning with the 2nd full week in September, 45/bay system (except 20 net sets in East Matagorda), no more than five and no less than three net sets/week/bay. Monofilament nets (183 m long; 1.2 m deep with 45.7 m sections of 7.6, 10.2, 12.7, and 15.2 stretched mesh tied together in ascending order) were set overnight, perpendicular to the shoreline with the 7.6 cm stretched mesh on the shoreward end, from randomly selected locations. Twenty estuarine bag seines (18.33 m wide, 1.8 m deep with 1.3 cm stretched nylon multifilament mesh in the 1.88 m wide central bag and with 1.9-cm stretched mesh in the remaining webbing) were pulled parallel to shore for 15.2 m at randomly selected locations in each major bay each month. Twenty otter trawls (6.1 m wide with 3.8 cm stretched nylon multifilament mesh) were pulled for 10 min in water ≥ 1.0 m depth at randomly selected locations in each major bay each month. Date, location, water depth (m), salinity (psu), water temperature (°C), and dissolved oxygen (mg L^{-1}) were recorded for each estuarine sample. Organisms caught were identified to the lowest taxonomic level (typically species), counted, and measured (total length in mm, TL, from the tip of the snout to the tip of the tail fully extended).

River fauna were sampled in September, October, November, and December 2017 at nine streams in the Upper Laguna Madre, Mission-Aransas Bay, San Antonio Bay, and Matagorda Bay watersheds. Sampling was performed using a multi-pass depletion method, consisting of three sampling passes using a backpack electrofisher (Smith Root LR-24) within a 75-m reach bounded by block nets (McGarvey et al. 2017). Organisms caught were identified to the lowest taxonomic level (typically species), counted, and the first 25 individuals of reach species were measured (fork length in mm, FL, from the tip of the snout to the tail fork fully extended). Depletion curves were applied to the three-pass abundance data to estimate total abundance of fish and crustaceans of each taxon within each reach (McGarvey et al. 2017). Fall 2017 data were compared to surveys in April 2017 and October 2016 to establish baseline numbers for expected faunal abundance.

Sedentary Biota

Mangroves were monitored at six sites as part of a long-term study on the mangrove-marsh ecotone (Guo et al. 2017). Each site was dominated by black mangroves, *Avicennia germinans*, with ~ 10% cover of saltmarsh plants, including *Batis maritima*, *Salicornia* and *Sarcocornia* spp., and *Spartina alterniflora*. At each site, a transect perpendicular to the shoreline was established, extending at least 42 m from the water-vegetation interface. In 1 × 1 m sub-plots along each transect, we recorded either mangrove presence/absence or a visual estimate of percent cover. Surveys were conducted in August 2015 and repeated after Harvey landfall in October 2017. For sites with presence/absence data, percent cover was estimated as the percent of sub-plots with mangroves present. At other sites, mangrove cover is reported as the average across all sub-plots.

Seagrass percent cover was sampled at 126 fixed stations across the southern and central Texas coast in the Mission-Aransas and Nueces estuaries in July and August 2017 prior to the impact of Hurricane Harvey as part of the Texas Statewide Seagrass Monitoring Program (texasseagrass.org). Within 10 m of the GPS coordinate designating a station, four replicate 0.25 m^2 quadrats were placed. Within each quadrat, the percent cover of each seagrass species was estimated with direct visual observation by a trained team of observers. Concurrent with each sampling, in situ measurements were made of a suite of chemical and physical environmental parameters including salinity. All 126 sampling stations were re-surveyed in September to October of 2017, and the absolute and proportional change in seagrass percent cover was recalculated. Maximum sustained wind gust data was collected from 70 weather stations to generate a raster of wind intensity for the coast. Interpolated wind speed values were extracted for each sampling station, and linear

regression was used to evaluate the relationship between absolute change in seagrass cover and maximum sustained wind gusts experienced.

Benthic macroinfauna sampling has been performed in the Guadalupe Estuary (i.e., San Antonio Bay) as part of long-term studies to identify the importance of freshwater inflow in controlling benthic dynamics (Montagna and Kalke 1992; Montagna and Kalke 1995; VanDiggelen and Montagna 2016). Four stations are aligned along the salinity gradient within the estuary from the freshest station (salinity 8.51 ± 0.48 SE) to the saltiest station (salinity 26.20 ± 2.15 SE). Macrofauna were sampled with a 6.7-cm diameter core tube (35.4 cm^2 area) to a sediment depth of 10 cm. Three replicates were collected per station twice prior to the storm (April and July 2017) and twice after the storm (October 2017 and January 2018). Organisms were extracted on a 0.5-mm sieve and enumerated to the lowest taxonomic level possible. Biomass was determined for higher taxonomic groupings by drying at 55 °C for 24 h.

Oyster dredges (Louisiana style 9-tooth; 46 cm wide, 25 cm tall with a 36-cm deep bag) were used to sample reefs from oyster-producing bays (Sabine Lake, Galveston, Matagorda, San Antonio and Aransas), 20 samples per month (except 30 per month in Galveston and 10 per month in Sabine). Dredges were pulled linearly at 3 knots h^{-1} for 30 s from randomly selected locations. Live and dead oysters were counted, and the percent live oysters were calculated for each sample. Pre-storm data were 4 months before Harvey, May–August; post-storm data are 4 mo after Harvey, September–December.

Sediments

Sediment cores (8 cm I.D. × 30 cm length) were collected in the Mission-Aransas Estuary by push-corer. Triplicate cores were collected at each site. The top 5 cm of each core was sectioned, and the rest was discarded; the top sections (0–5 cm from surface) from the triplicate cores were combined and homogenized in a plastic storage bag and stored in a cooler on ice until return to the lab on the same day. Sediment samples were then freeze dried and screened with a 300-μm mesh to remove large debris and shells.

Sediment grain size was measured using a laser diffraction particle size analyzer (Beckman-Coulter LS 13320). About 15–20 mL of hydrogen peroxide (1:2) were added to ~0.2 g of sediment in a beaker. After incubating for 24 h at 40 °C to remove organic matter, sodium hexametaphosphate $[(NaPO_3)_6]$ was added to the sediment and mixed for 15 min in an ultrasonic bath to aid disaggregation. The size distribution was measured by polarization intensity differential scattering. The detection size range of this analyzer is from 0.02 to 2000 μm.

Statistical Analyses

Resistance was calculated as the natural log of the maximum or minimum post-storm value divided by the baseline value (hereafter referred to as the log response ratio or LRR). Resilience was calculated as the number of days until values returned to baseline. Baseline was calculated as the mean value immediately before Hurricane Harvey in the case of spatially replicated data or the mean value for August in the case of temporally replicated data. In the case of responses which did not return to baseline, all values were assigned the same value (140 days) to eliminate variation caused by differences in sampling frequency. All analyses were conducted using the statistical program R version 3.4.3 (R Core Team 2016). To evaluate the relationship between resistance (LRR) and resilience (return time), the LRR of the absolute value of the deviation from baseline was regressed against the return time using quantile regression. Absolute value was chosen to focus the analysis on the magnitude rather than the direction of the response. Quantile regression was chosen to evaluate the relationship between resistance and resilience because multiple factors may simultaneously impact resistance driving variation in response magnitude, but there is a physical limit on the potential magnitude of a response (Gotelli and Ellison 2013). Two quantile regression models, tau of 0.9 (high slope) and tau of 0.5 (no slope), were compared to evaluate the existence of the relationship using ANOVA in the *quantreg* package (Koenker 2018). Differences in resistance and resilience among response categories were evaluated using ANOVA followed by a Tukey-HSD post-hoc test. Tests for temporal changes were evaluated as mixed effects models using the *lme()* function in the *nlme* package with site identity treated as a random effect with an autocorrelation structure of order 1 (Pinheiro et al. 2017). Changes between paired time points in significant temporal series were evaluated using *t* tests. PERMANOVA was used to test for changes in community composition between time points using the *vegan* library (Oksanen et al. 2014).

Results

Resistance and Resilience Among Ecosystems

We observed a negative relationship between the LRR of the absolute value of the deviation from baseline (resistance) and the time to return to baseline (resilience) across response variables (slope = − 0.018, $F = 9.732$, DF = 1, $P = 0.002$; Fig. 2a). The response magnitudes within ecosystem components were similar across different ecosystems (Fig. 2b, c). Hydrologic and hydrographic variables in both the rivers and estuaries displayed the highest magnitude shifts from pre-storm conditions representing relatively low resistance to disturbance

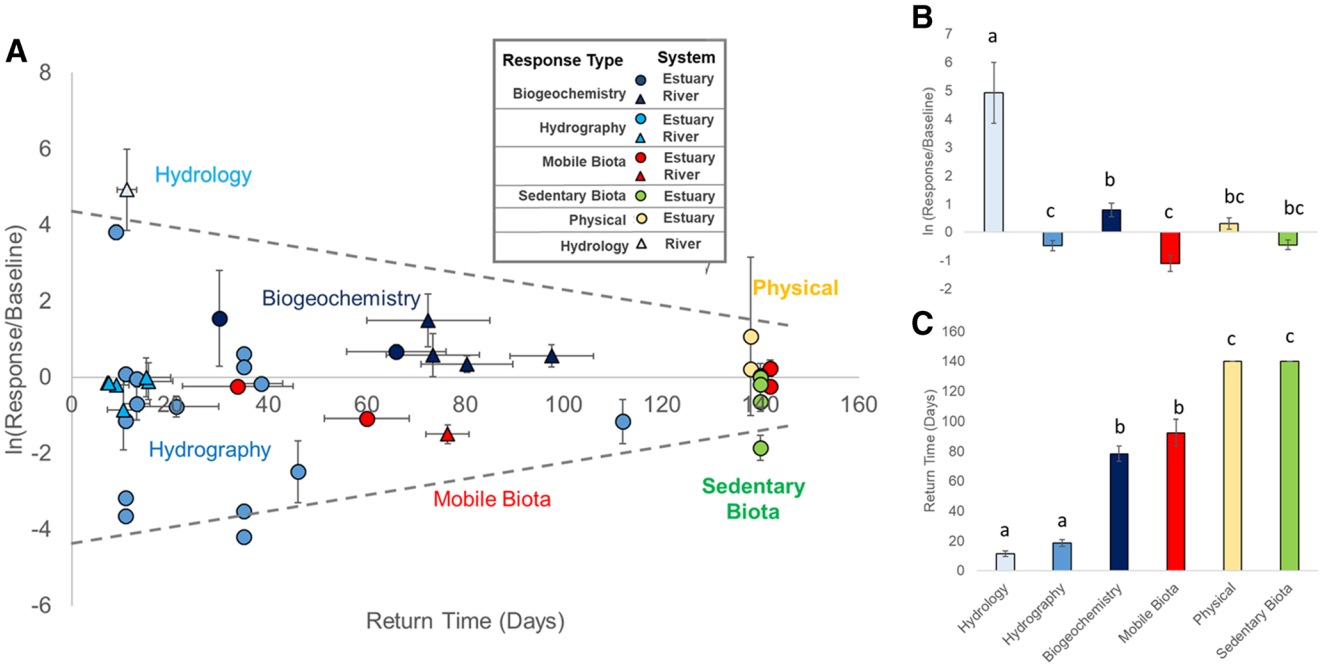

Fig. 2 Hurricane Harvey resistance—resilience synthesis. **a** The *X*-axis is the return time to baseline conditions in days, representing system resilience (systems which had not returned to baseline were assigned a value of 140 days to avoid biases due to variation in sampling frequency). The *Y*-axis is log response ratio (LRR), the natural log of the maximum response divided by the baseline value, representing system resistance. Each symbol represents a time series of a particular response for a particular ecosystem type. Symbols with error bars (standard error) had multiple spatial locations with the time series. Symbol shape represents system type (triangle = river; circle = estuary), and symbol color represents the ecosystem response type (dark blue: biogeochemical, e.g., nutrients, carbon flux, chlorophyll-a; blue: hydrographic, e.g., oxygen, temperature, pH, salinity; light blue: hydrologic, e.g., river discharge; red: mobile fauna, e.g., invertebrates and fish; green: sedentary fauna, e.g., plants and benthic invertebrates; yellow: physical, e.g., sediment grain size, TSS). The dotted lines are the quantile regression lines (tau = 0.9, $P < 0.001$). B) The average LRR ± SE for each response type. **c** The average return time to baseline in days ± SE for each response type. For **b** and **c**, letters over bars denote statistically significant differences among response types based on a Tukey-HSD post-hoc test following a significant one-way ANOVA

(Fig. 2a, b). However, hydrographic conditions returned to pre-storm levels significantly faster than other ecosystem attributes (mean ± SE = 18.56 ± 21 days, $P < 0.005$; Fig. 2a, c), indicating these system properties had the highest resilience. Biotic variables generally displayed negative responses to wind and rain with higher resistance in sedentary biota as compared to mobile biota. The mobile biota within the rivers and estuaries, however, were more resilient than sedentary biota (Fig. 2c; $P < 0.001$).

Hydrology

River discharge in streams and rivers within the region increased by 264 to 103,600%, within a few days of the storm. The responses were the highest magnitude of any variable in the dataset. The highest discharge events occurred to the east of landfall, following the asymmetric pattern of precipitation associated with the storm (Fig. 1). Northeastern sites that received more rainfall took longer to return to pre-storm flow conditions (Fig. 3a), while southwestern sites that received less rain returned to pre-storm flow conditions more rapidly (Fig. 4a).

Hydrography

Response magnitude and return time were highly variable among hydrographic variables. The response magnitudes and return times were higher in the estuaries than in the rivers. This can largely be attributed to differences in water residence time, with shorter residence time related to faster return time. Salinity in San Antonio Bay initially quadrupled over a 12-h period (from 7.39.6 ± 0.03 SE to 32.09 30.9) due to storm surge and then dropped over the following 5 days due to increased discharge from the Guadalupe River. Low salinity conditions (< 5 ppt) lasted for over 1 month in San Antonio Bay (Fig. 5). Within Copano Bay, salinity dropped from 18.9 to 3.3 ppt from rain and river discharge (Fig. 3a), and low salinity conditions took > 7 months to return to pre-hurricane levels, indicating low resilience (Fig. 3b). In Copano Bay, turbidity increased due to resuspension of fine material from wave action and surge, peaking at > 1300 NTU, the highest recorded level since the sensors were installed in 2007, but this increase in turbidity lasted only 2 days (Fig. 3a). Two days after the storm made landfall, there was a secondary peak in turbidity (following a prior peak associated with storm surge) associated with riverine run-off (Fig. 3a).

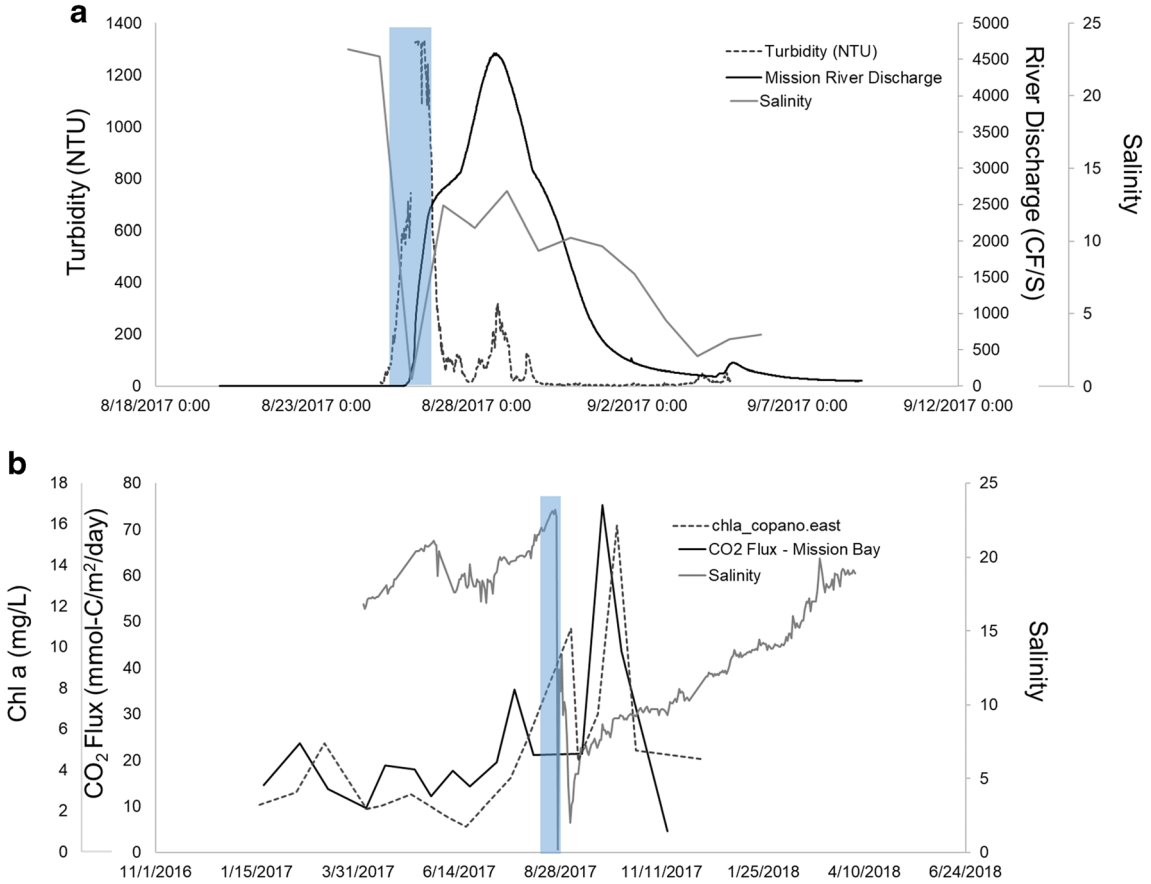

Fig. 3 Storm impacts on the Mission-Copano Bay estuary. **a** Time series of Mission River discharge (thick black) and salinity (thin black) and turbidity (dashed) in the receiving estuary. **b** Time series of chl a (dashed), CO_2 flux (thick black), and salinity (thin black) in Copano and Mission bays. Blue bars indicate the period of the hurricane

Dissolved oxygen concentrations varied among rivers, with bottom water anoxia occurring in rivers that experienced high discharge and loss of diel cycling for 5–18 days after the hurricane passed. Following resumption of diel cycling, the amplitude of the diel oxygen cycle was reduced by 44% (2.3 ± 4.7 mg L^{-1}). For example, in the Aransas River, average maximum and minimum DO dropped from 7.47 ± 1.54 to 3.27 ± 1.78 mg L^{-1} and 1.95 ± 0.49 to 0.44 ± 0.16 mg L^{-1} respectively, for 7 days after the storm. Within the San Antonio Bay estuary, concurrent with the onset of high river flow and low salinity conditions (Fig. 5a), hypoxic and anoxic conditions formed at the bottom and near the surface. Hypoxic conditions persisted for approximately 8 days in near-surface and bottom waters simultaneously (Fig. 5b).

Biogeochemistry

Biogeochemical responses in both the rivers and estuaries were all positive and were an intermediate magnitude relative to other responses (Fig. 2). Responses generally returned to pre-storm levels quickly; however, NO_3^- and TDN (total dissolved nitrogen) in the rivers were an exception. NO_3^- and TDN continuously increased post-storm, rising more than 300% in some systems and remaining elevated. For example, NO_3^- concentrations reached 14.26 ± 0.46 mg L^{-1} in the Aransas River by December 2017 ($df = 1,4$, $P = 0.0005$). Ammonium concentrations were not affected by the storm ($df = 1,4$, $P = 0.763$). Orthophosphate concentrations within rivers increased immediately after the storm and then returned to pre-storm levels within a month ($df = 1,4$, $P = 0.0004$). Concentrations of orthophosphate increased by as much as 1300% in some systems, reaching as high as 8.83 ± 1.26 mg L^{-1}. However, nutrients including NO_3^-, NH_4^+, and orthophosphate remained at low levels in Copano and Aransas Bays on September 13 (first sampling date after the hurricane) until December 2017. During this period, chlorophyll-a concentration (a proxy for total phytoplankton biomass) increased relative to pre-storm conditions (June 2017; Fig. 3b).

Fig. 4 Storm impacts on the Aransas River. **a** High-frequency time series of dissolved oxygen (gray), temperature (thin black), and river discharge (thick black). **b** Synoptic sampling of NO_3^-, DOC, and orthophosphate from August to December 2017. Data show pattern of elevated nutrients and a temporary elevation in DOC following the storm. Error bars are standard error. **c** Synoptic sampling of conductivity and pH for the aforementioned period. Data show a pattern of dropping conductivity and increasing pH with the precipitation event. Blue bars indicate the period of the storm

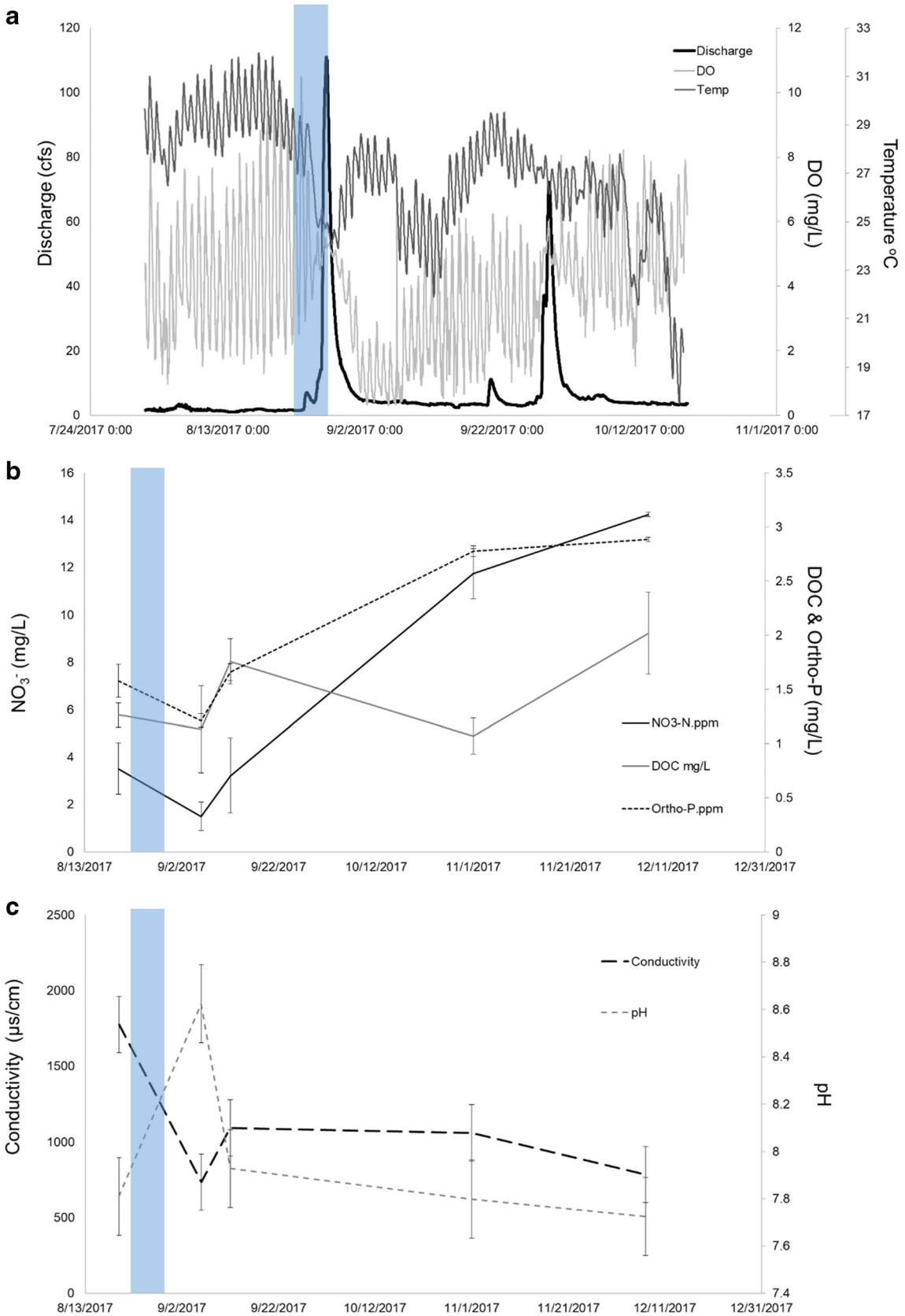
a
Discharge (cfs)
DO (mg/L)
Temperature °C
Discharge
DO
Temp
7/24/2017 0:00
8/13/2017 0:00
9/2/2017 0:00
9/22/2017 0:00
10/12/2017 0:00
11/1/2017 0:00
b
NO3- (mg/L)
DOC & Ortho-P (mg/L)
NO3-N.ppm
DOC mg/L
Ortho-P.ppm
8/13/2017
9/2/2017
9/22/2017
10/12/2017
11/1/2017
11/21/2017
12/11/2017
12/31/2017
c
Conductivity (µs/cm)
pH
Conductivity
pH
8/13/2017
9/2/2017
9/22/2017
10/12/2017
11/1/2017
11/21/2017
12/11/2017
12/31/2017

Within the rivers, DOC (dissolved organic carbon) increased immediately after the hurricane with concentrations rising more than 250%, reaching as high as 26.35 mg $L^{-1} \pm 0.412$ SD in some systems before declining again ($df = 1,4$, $P < 0.001$). Within the estuaries, CO_2 fluxes to the atmosphere also shifted, and similar to DOC fluxes, the response was variable across bay systems. In "normal" years, water-to-air CO_2 flux in San Antonio Bay is 98.4 mmol-C m^{-2} day^{-1} (Yao et al. 2020). An extreme increase in pCO_2 levels 1 month after the disturbance led to nearly 50% increase in CO_2 flux on an annual scale (144.5 mmol-C m^{-2} day^{-1}) (Fig. 5a). San Antonio Bay then quickly changed from a CO_2 source to a sink in October (uptake of CO_2 from the atmosphere), consistent with previous multiyear observations, indicative of returning to "normal" estuarine conditions for this time of the year. In contrast, the adjacent Mission-Aransas Estuary saw a decrease in CO_2 flux (14.7 mmol-C m^{-2} day^{-1}) after the hurricane.

Mobile Biota

Mobile biota responses to and recovery from the storm differed between riverine and estuarine assemblages. Across all rivers, fish and crustacean abundance were reduced by 62–95% after the hurricane (Fig. 6a). In some coastal rivers, fish and crustacean biodiversity was also reduced and composition shifted toward abundant estuarine species such as anchovy (*Anchoa mitchilli*) and daggerblade grass shrimp (*Palaemonetes pugio*). Abundances of riverine fish and crustaceans recovered to pre-storm levels by November 2017 ($df = 1,3$, $P < 0.0001$). In contrast, when comparing estuarine gill net data from pre-storm to post-storm periods (Fall 2016 vs. Fall 2017), there were minor shifts in fish community structure in all Texas estuaries except the Laguna Madre (see Supplementary Material). Monthly seine data from July 2017 to December 2017 showed a typical seasonal pattern of fish and crustacean abundance significantly declining until October and then rebounding with the arrival of the fall recruits ($df = 1,5$, $P = 0.003$; Fig. 6b; Nelson 1992). The reduced catch per unit effort (CPUE) from August to September 2017 was larger ($df = 9,32$, $P = 0.01$) in Aransas (−74%), San Antonio (−66%), Corpus Christi Bay (−40%), and Upper Laguna Madre (−36%) than is typical from the previous 6-year period (2010 to 2016 mean change in CPUE from August to September for Aransas Bay −31% ± 11 SE, San Antonio

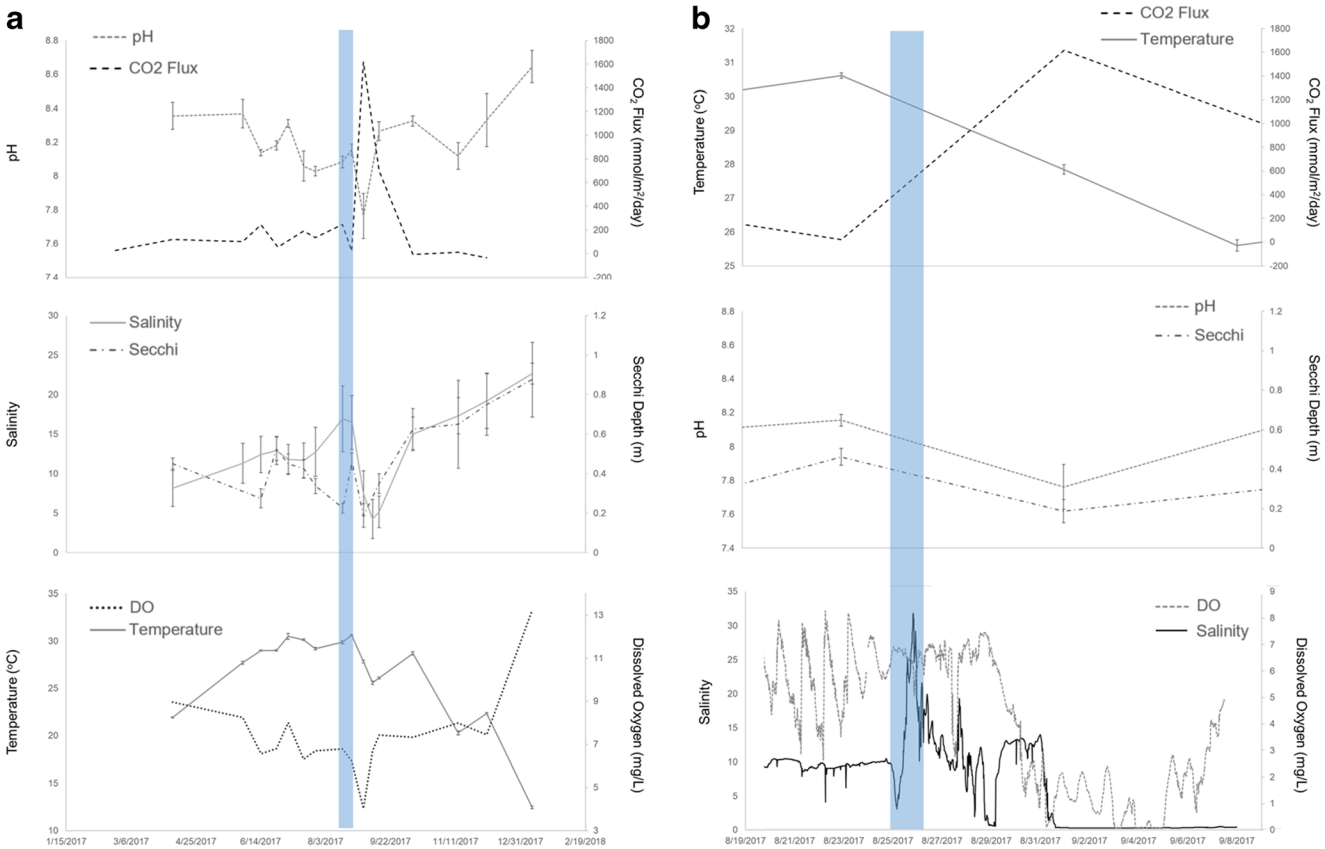

Fig. 5 Storm impacts on San Antonio Bay. **a** Synoptic sampling for pH, CO_2 flux, salinity, secchi depth, dissolved oxygen, and temperature from spring 2017 to winter 2018. Data show the increase in CO_2 flux followed by rapid drop and temporary dips in pH, salinity, secchi depth, dissolved oxygen, and temperature. Error bars are standard error. **b** Synoptic and high-frequency data from mid-August to early September 2017. Salinity dropped to nearly zero for days after the storm while bottom dissolved oxygen levels became anoxic 5 days post-hurricane and remained anoxic for another 8 days. Blue bars indicate the period of the hurricane

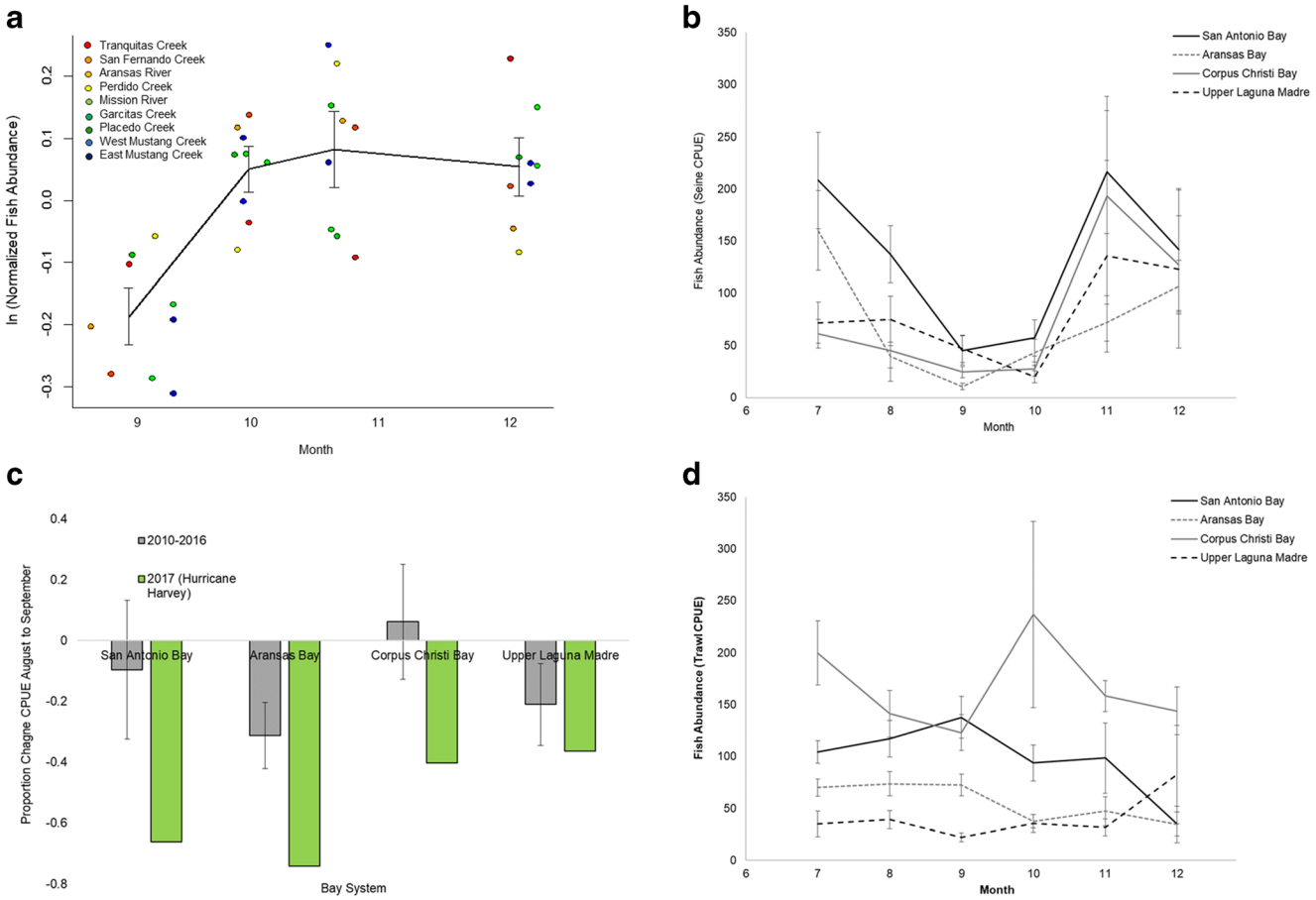

Fig. 6 Mobile fauna responses. **a** Natural log of normalized fish and crustacean abundance in each stream reach from September to December 2017. Black line is the mean across sites, error bars are standard error. **b** Mean fish and crustacean abundance (CPUE) in seine hauls for select estuaries from July to December of 2017. **c** Proportional change in fish abundance in seine hauls from August to September for select estuaries from 2010 to 2016 (gray bars) and 2017 (green bars). **d** Mean fish and crustacean abundance (CPUE) in otter trawls for July to December of 2017

Bay − 10% ± 23 SE, Corpus Christi Bay 6% ± 19, and Upper Laguna Madre − 21% ± 13; Supplement 2G).

Sedentary Biota and Physical Responses

Sedentary taxa, including vegetation and sessile benthic taxa, all exhibited negative but low-magnitude responses to the disturbance; however, return times were the highest among measured responses (beyond the duration of the current study). In the coastal wetlands just south of the storm track, black mangrove (*A. germinans*) cover dropped 25–40%. The decline in mangrove cover was largely due to loss of upper foliage, though some trees were killed after being entirely uprooted and displaced. Foliage on lower branches remained largely intact, likely because the lower branches were protected from the wind by submersion via storm surge.

The strongest winds were within the Mission-Aransas Estuary, which resulted in physical removal of seagrass. There was a negative relationship between absolute change in percent cover of turtle grass (*Thalassia testudinum*) seagrass and maximum sustained wind gusts experienced at a site ($R^2 = 0.15$, slope = − 0.18). Overall, 12% of stations with *T. testudinum* present pre-storm lost 100% of *T. testudinum* cover post-storm and 30% of stations lost at least 50% of pre-storm cover. These severe declines were only in areas that experienced category 3 or category 4 force winds (178–251 km h^{-1} sustained wind speed). As noted by Congdon et al. (2019), seagrass damage included both complete removal (roots/rhizomes ripped from the sediment) and partial removal (aboveground biomass sheared off). In areas where rhizome material remained intact, regrowth of above ground tissue occurred within 1–3 months (pers. obs., VMC).

Many benthic estuarine faunal assemblages exhibited negative responses to the storm event. There was significant difference in percent live oysters among months in Aransas Bay between July and December 2017 (df = 5,104, $P = 0.0334$). The largest drop in live oyster cover occurred between August (pre-storm; 54%) and September (post-storm; 22%).

In San Antonio Bay, benthic macroinfaunal diversity ($P < 0.0001$, df = 15,32), abundance ($P < 0.0001$, df = 15,32), and biomass ($P < 0.0001$, df = 15,32) all declined significantly after the storm. Four months prior to the storm in April 2017, abundance was as high as 53,900 individuals m^{-2}. Following the storm, abundance dropped to 9800 individuals m^{-2} in October 2017 and remained low (9400 individuals m^{-2}) through January 2018. The biomass of the macroinfauna declined from a maximum of 38.6 g m^{-2} in July 2017 to a maximum of 6.1 g m^{-2} in October and 1.7 g m^{-2} in January 2018. Benthic macroinfaunal species richness declined from a maximum of 10.3 species/core prior to the storm to 3.3 species/core in October 2017 and then increased to 6.7 species/core in January 2018. The declines were due to losses of 22 of the 49 species found. However, the greatest losses were for the polychaetes (*Mediomastus ambiseta*, *Streblospio benedicti*, and *Capitella capitate*), oligochaetes, and the mollusks (*Rangia cuneata* and *Macoma mitchelli*). Post-storm, the benthic macroinfauna community composition shifted, and recovery was driven by a recruitment event of juveniles in January and April 2018 of the mollusks *Texadina sphinctostoma* and *Mulinia lateralis*, and the polychaeta *Spiochaetopterus costarum*.

Several changes in the estuarine edaphic (sediment) characteristics in Mission-Aransas Bay followed the storm. Median grain size in surface sediments (0–5 cm) increased as much as 100 μm at a sampling site near Harbor Island after the hurricane. Benthic chlorophyll-a concentrations declined, possibly resulting from wind-induced scouring or burial. There was also a large drop in the percentage of benthic pheophorbide from 15 ± 6% in June 2017 to 4 ± 2% in October 2017. Pheophorbide concentrations approached pre-storm baseline levels by January 2018 (12 ± 5%).

Discussion

We present one of the most comprehensive syntheses of impacts of a major hurricane on coastal systems to date, in terms of the geographic extent of systems examined and the breadth of response variables. The analyses reveal an important pattern of negative covariance between resistance and resilience among ecosystem components. Hydrographic and biogeochemical components of the system, while displaying some of the largest magnitude changes from pre-storm condition (low resistance), returned to baseline quickly (high resilience). Even though the influx of freshwater and nutrients was large, rivers and estuaries are dynamic systems and thus may be able to buffer and absorb these types of disturbances. In contrast, although structural components of ecosystems such as seagrasses, mangroves, and oyster reefs were overwhelmingly more resistant to disturbance than factors like water chemistry and mobile fauna, recovery time for these structural components can take years or even decades (Ilg et al. 2008; Levin 1984; Lytle et al. 2008). These patterns and the observed resistance/resilience covariance enhance our understanding of how tropical cyclones impact coastal systems. Furthermore, our analysis framework is flexible and can be used in future studies to measure and compare hurricane responses across abiotic and biotic variables.

Hurricane Harvey impacted coastal ecosystems through both the intense wind and storm surge disturbance which lasted less than 24 h within the study region, and through record-breaking rainfall leading to large amounts of runoff, which ultimately altered salinity and chemical conditions. Although there were interactions between wind- and rain-driven disturbances, many responses within biological, hydrographic, and biogeochemical components are most likely attributed to one or the other. Furthermore, there was spatial separation in the major impact zone of the physical and rain-driven disturbances, which facilitated examination of the effects of each of those drivers. Many of the responses by flora and fauna can be attributed to the immediate impact of physical disturbance, but the drivers differed among groups. For example, scouring from rain induced floods likely impacted riverine mobile fauna, whereas scouring resulting from high winds impacted estuarine macrofauna and seagrasses. In contrast, many of the shifts in hydrographic, hydrologic, and biogeochemical variables were likely largely driven by the rainfall event. We examine these drivers and responses below.

Impacts of the storm on physicochemical responses varied both spatially and between estuarine and freshwater systems, we discuss each of these in turn. Riverine concentrations of most dissolved solutes, in particular nutrients and DOC, increased for only a short period of time after the storm. These findings are consistent with those predicted by the Pulse-Shunt Concept, which states that major hydrologic events drive the timing and flux of terrestrial DOM to aquatic ecosystems (Raymond et al. 2016). When water tables rise during storm events, organic matter is leached from soils and flushed into streams and rivers (Boyer et al. 1997; Hornberger et al. 1994). Differences in the yields of DOC from watersheds in response to Hurricane Harvey are likely driven by a combination of land use, topography, and antecedent conditions (McMillan et al. 2018). Wetlands and topographic depressions are sources of DOC within watersheds that can be flushed during storm events (Creed et al. 2003; Richardson et al. 2010). The flux of landscape sources of DOC downstream is also driven by the degree to which a flood event increases surface water connectivity of upland DOC sources to streams and rivers (Hosen et al. 2018). Ultimately, much of the terrestrial organic matter mobilized during extreme weather events such as Hurricane Harvey is delivered to coastal ecosystems where it enhances heterotrophic microbial respiration (Crosswell et al. 2014; Watanabe and Kuwae 2015).

The observed impact of the storm on riverine NO_3^- concentrations, which increased and remained elevated for months after the storm, was significantly different from responses of other solutes. The observed pattern mirrors the effect of Hurricane Hugo on stream water chemistry in Puerto Rico, where NO_3^- concentrations increased 4-fold in response to the storm and remained elevated for 12–18 months (Schaefer et al. 2000). Reduced nutrient uptake in the terrestrial environment due to loss of aboveground vegetation during the storm combined with leaching from downed litter is potentially responsible for the prolonged elevation of water column nutrient concentrations (Schaefer et al. 2000). Increased nutrient loading into streams from hurricanes often results in higher dissolved nutrient concentrations in the estuarine water column (Wachnicka et al. 2019). NO_3^- is particularly prone to elevated concentrations because other forms of dissolved nitrogen rapidly convert to NO_3^-, and positive phosphorus ions are likely to be bound to negatively charged sediment particles. However, following Harvey, the receiving estuaries showed no such prolonged elevation in dissolved nutrient concentrations despite the increased nitrogen load. This phenomenon could be attributed to rapid uptake by phytoplankton. Overall, chlorophyll-a concentrations were elevated relative to previous years, where the maximum concentrations are typically observed during the summer (Reyna et al. 2017). In particular, diatoms, a dominant group in Aransas and Copano Bays (Anglès et al. 2015), are known to respond rapidly to elevated nutrient input (Colos 1986; Pinckney et al. 1999). Taxa common in this region can bloom after freshwater inflow events (Anglès et al. 2015) and subsequently cause a rapid decrease in nutrient concentrations during blooms (Popovich et al. 2008).

Differences in response magnitudes among the different estuaries can likely be attributed to variation in the amount of rainfall received and/or the differences in geomorphology of the basins contributing to variation in water residence time. For example, the difference in CO_2 flux between Mission-Aransas Bay and San Antonio Bay can be attributed to spatial variation in rainfall. In San Antonio Bay, enhanced CO_2 flux post-storm was likely a combination of enhanced respiration of river-transported terrestrial DOC and river water degassing because of high DIC concentrations. The Mission-Aransas Estuary showed more of local precipitation influence, as dilution of seawater increases CO_2 solubility (Yao and Hu, 2017), and local runoff may have flushed nutrients from the watershed into the bay, fueling primary production. However, the intensity of the rainfall effects was modulated by estuary residence time. Where residence time was longer, the impacts had a greater magnitude, and effects persisted for longer periods of time. For example, Aransas Bay and Copano Bay (part of the Mission-Aransas Estuary system) received similar amounts of rainfall but had different freshwater inflow impacts. The 7-month period of low salinity in Copano Bay (compared to 1 month in Aransas Bay) following the storm can be attributed to its ~ 1.5-year residence time (Solis and Powell 1998). High levels of precipitation combined with long water residence time may have cascading impacts on other ecosystem properties that are less resilient. For example, bottom water hypoxia (dissolved oxygen concentration less than 2 mg L^{-1}) in conjunction with low salinities likely drove losses in estuarine benthic infauna, which took longer to recover.

In general, fauna (mobile and sedentary) were among the more resistant components of the system evaluated. This resistance may be explained by a combination of adaptation to environmental fluctuations and, in the case of mobile fauna, the ability to move to avoid them. Estuaries and rivers are inherently dynamic environments and thus associated fauna are often adapted to respond to large swings in environmental conditions, like salinity or scouring floods, making estuarine and riverine fish and crustaceans less vulnerable to disturbance events (Frid and Townsend 1989; Townsend 1989). For example, estuarine fish typically exhibit a high tolerance for salinity fluctuations (Nordlie 2003). Mobile fauna showed higher resilience to disturbance than sedentary fauna, suggesting dispersal/movement ability may be key in mediating organismal responses. This is further supported by the observation that recovery intervals were shorter (weeks–months) than the reproductive cycle of many of these taxa (annual). This suggests that mobile biota were able to move out of affected areas and/or recolonize the systems quickly (Bell and Eggleston 2005; Massie et al. this volume). However, we did not evaluate whether mobile fauna had higher tolerance to environmental fluctuations than sedentary fauna, and so the mechanism behind the observed differences requires further evaluation.

Seasonal recruitment dynamics may have also played a role in rapid recovery of mobile fauna. For example, there is typically a drop in the abundance of estuarine fish in early fall in these systems followed by an increase with the arrival of the fall recruitment class for some species (Heck et al. 2003; Reese et al. 2008). The results from nearshore seine data suggest that the storm may have exacerbated the natural seasonal cycle, causing a larger dip than usual, but the effects were short-lived (Fig. 6c). The seasonal arrival of fall recruits may have contributed to the rapid recovery in estuarine fish populations; however, this was likely not the only mechanism. Trawl data from these same systems within open waters showed no temporal patterns (Fig. 6d), suggesting that high wave energy and tidal shifts concentrated the storm impacts on mobile fauna along the shorelines. Therefore, recolonization to the nearshore zone may have also come from populations that sought refuge in open water during or preceding the storm. These observations contrast with those made in Florida Bay after Hurricane Irma, where the relative abundance of many fish species declined by more than 50%, and pre- and

post-storm assemblages were substantially dissimilar, largely due to increases in anchovies and declines in mojarra and killifish (Zink et al. this volume). In the rivers, there was an increase in estuarine fauna and secondary freshwater fishes immediately after the storm before returning to a state dominated by primary freshwater fauna. These taxa may have been pushed up into the streams by the storm surge or could have colonized quickly from refugia in the downstream estuary.

Sedentary biota (fauna and flora), in contrast, could not actively avoid stressful physical (high wave energy) or hydrographic (low dissolved oxygen) conditions, and recolonization may take longer, as it likely requires dispersal of new recruits or vegetative growth into denuded areas. Dynamics in these groups were most likely a function of taxa-specific life history characteristics and disturbance intensity. For example, impacts on estuarine benthic sedentary biota can be attributed to low salinity and anoxia such as the effects of low salinity and bottom anoxia resulting from freshets on oyster mortality (Munroe et al. 2013), as was observed in Galveston Bay following Hurricane Harvey. However, significant physical disturbance from storm surge has the potential to directly damage oyster reefs, and this is the likely explanation for declines in live oysters in Aransas Bay following the storm, as salinities (> 5) were not low enough (< 3.5) for sufficient time to elicit oyster mortality (Galtsoff 1964; La Peyre et al. 2009).

Saltmarsh grasses were largely resistant to physical impacts, likely because these low-stature, flexible plants were either submerged or were able to lie flat when the wind was strong (Armitage et al. 2019). In contrast, the taller, more rigid mangroves suffered greater defoliation; this damage pattern is typical in many tropical mangrove species (Branoff this volume). This pattern of damage is characteristic of major wind events, and is typically constrained to the area near the landfall of the storm's eye with the highest wind speeds (Armentano et al. 1995; Smith et al. 2009). Mangrove stands on the Texas coast are dominated by a single rapidly growing species, *A. germinans* (Tomlinson 2016). Storm damage to the upper branches *A. germinans* was followed by rapid resprouting of leaves within 2 months of the storm, though complete canopy recovery may take multiple growing seasons (Armentano et al. 1995). Similar patterns of damage and rapid recovery in *A. germinans* followed Hurricane Andrew in Florida in 1992 (Baldwin et al. 2001; Smith et al. 1994). *Avicennia germinans* is relatively resilient to these types of disturbances, and even complete defoliation does not necessarily result in tree mortality (Imbert et al. 2000; Roth 1992).

Recovery of seagrasses will likely differ substantially than that for mangroves because in many cases, whole plants were uprooted (Congdon et al. 2019). One of the two dominant seagrass species in our region, *T. testudinum*, has one of the slowest rhizome elongation rates among Atlantic seagrasses (Duarte 1991), which may further slow recovery of disturbed areas when its rhizomes are physically disturbed or the beds are buried by storm sediment deposition (Hernandez-Delgado et al. this volume). Recovery of *T. testudinum* in areas that have experienced physical disturbance from boat groundings has been observed to be 2 to 7 years (Bourque et al. 2015; Zieman 1976), and many disturbed areas from Harvey are of an even larger spatial extent (Congdon et al. 2019). However, sexual reproduction and seed recruitment may enhance recovery (Whitfield et al. 2004) and sexual reproductive effort is high in *T. testudinum* seagrass beds in South Texas (Kaldy and Dunton 2000).

Looking across mobile and sedentary biota, the results imply that the greatest long-term impacts occurred on sedentary biota. This phenomenon has been observed in other systems following extreme events, such as the catastrophic impact of Hurricane Agnes on Chesapeake Bay in 1972, where mobile fauna recovered quickly after the storm, but submersed aquatic vegetation took decades to recover (Orth and Wilcox 2009). Prolonged recovery trajectories of sedentary biota are often linked to habitat fragmentation and small patch size. In forest responses to hurricanes, fragmentation led to negative feedback loops once extreme events occur in the system (Laurance and Curran 2008). Looking to marine systems, seagrasses self-buffer against perturbations once a critical patch size is reached (Gruber et al. 2011; Orth et al. 2017; van der Heide et al. 2011), and similar processes likely operate on oyster reefs (Moore et al. 2018) and mangrove stands (Huisman et al. 2009). The integrity of structural habitat has cascading positive effects on sediment accretion and shoreline stability, potentially promoting recovery to pre-storm conditions. The implications are clear—management actions to conserve large swathes of structural habitat may be key to enhancing overall coastal ecosystem resilience, and management interventions to restore structural habitat may be critical to promote rapid recovery of coastal ecosystems following major storms.

Considering all responses, we propose a general conceptual model that resistance and resilience in coastal ecosystems is a product of the relative influence of physical and biological constraints on the response variable of interest and that these are hierarchically arranged with biological constraints following physical constraints. For example, the majority of conservative solutes (not subject to uptake by the biota) returned to pre-storm levels rapidly via settlement and open ocean exchange; however, there were noted deviations from this general pattern. Systems with high residence time remained perturbed for longer periods, reflecting the physical constraint that basin morphology can exert on water movement. Similarly, the observation that riverine NO_3^- concentrations increased over time and remained elevated may reflect the biological control that watershed vegetation, which requires months to years to re-grow post-storm, exerts on riverine NO_3^- concentrations through uptake (Likens et al. 1970; Schaefer et al. 2000). In contrast, intermediate levels of

resilience in estuarine biogeochemical responses likely reflect the population cycling of phytoplankton, which is comparatively much vaster than terrestrial vascular plants (Laws 2013). This extends further to biological responses where, provided environmental conditions are suitable, recolonization and recovery must be a function of dispersal ability, distance to source populations, and generation times (Levin 1984; Lundquist et al. 2010).

Examining the impacts of Hurricane Harvey provides us with an opportunity to forecast how ecosystems along the coastline will respond to future hurricanes. We found opposing spatial gradients in the two major forms of disturbance associated with the storm; rain-driven effects, which were more pronounced in rivers and within the upper estuaries to the northeast of landfall, were spatially decoupled from wind effects, which were most pronounced near the landfall location on the coast. The analysis of Hurricane Harvey displays how variation in the identity of storm stressors and ecosystem components dictates the magnitude of the immediate and long-term impacts on coastal ecosystems. The intensity, high rainfall totals, and climatic conditions of the impact zone are all characteristics of predicted future storm scenarios for the US Gulf of Mexico and Atlantic coasts (Emanuel 2017; Seager et al. 2007; Seager et al. 2013). Thus, the impacts of Hurricane Harvey may be a preview of the new normal of hurricane impacts and responses in these regions.

Funding Information This material is based upon work supported by the National Science Foundation under Grant Numbers 1903760, 1760006, 1761677, 1761414, 1761428 1763167, 1807143, 1761444, and 1654232; by National Oceanic and Atmospheric Administration (NOAA) under award NA15NOS4780185; by support from the Texas College Research Enhancement Fund; by the ongoing sampling efforts of the Texas Parks and Wildlife Department; and by an Institutional Grant (NA14OAR4170102, NA18OAR4170088) to the Texas Sea Grant College Program from the National Sea Grant Office, NOAA, U.S. Department of Commerce.

References

Adger, W.N., T.P. Hughes, C. Folke, S.R. Carpenter, and J. Rockström. 2005. Social-ecological resilience to coastal disasters. *Science* 309 (5737): 1036–1039.

Anglès, S., A. Jordi, and L. Campbell. 2015. Responses of the coastal phytoplankton community to tropical cyclones revealed by high-frequency imaging flow cytometry. *Limnology and Oceanography* 60: 1562–1576.

Armentano, T.V., R.F. Doren, W.J. Platt, and T. Mullins. 1995. Effects of Hurricane Andrew on coastal and interior forests of southern Florida: overview and synthesis. *Journal of Coastal Research*: 111–144.

Armitage, A.R., C.A. Weaver, J.S. Kominoski, and S.C. Pennings. 2019. Resistance to hurricane effects varies among wetland vegetation types in the marsh-mangrove ecotone. *Estuaries and Coasts*.

Avery, G., R. Keiber, J. Willey, G. Shank, and R. Whitehead. 2004. Impact of hurricanes on the flux of rainwater and Cape Fear River water dissolved organic carbon to Long Bay, southeastern United States. *Global Biogeochemical Cycles* 18: 3015.

Baldwin, A., M. Egnotovich, M. Ford, and W. Platt. 2001. Regeneration in fringe mangrove forests damaged by hurricane Andrew. *Plant Ecology* 157: 151–164.

Bell, G.W., and D.B. Eggleston. 2005. Species-specific avoidance responses by blue crabs and fish to chronic and episodic hypoxia. *Marine Biology* 146: 761–770.

Bourque, A.S., W.J. Kenworthy, and J.W. Fourqurean. 2015. Impacts of physical disturbance on ecosystem structure in subtropical seagrass meadows. *Marine Ecology Progress Series* 540: 27–41.

Boyer, E.W., G.M. Hornberger, K.E. Bencala, and D.M. McKnight. 1997. Response characteristics of DOC flushing in an alpine catchment. *Hydrological Processes* 11: 1635–1647.

Branoff, B.L. this volume. Changes in mangrove tree mortality, forest canopy, and aboveground biomass accumulation rates following the 2017 Hurricane season in Puerto Rico and the role of urbanization. *Estuaries and Coasts*.

Colos, Y. 1986. Time-lag algal growth dynamics: biological constrains on primary production in aquatic environments *Marine Ecology Progress Series* 33.

Congdon, V.M., C. Bonsell, M.R. Cuddy, and K.H. Dunton. 2019. In the wake of a major hurricane: differential effects on early vs. late successional seagrass species. *Limnology and Oceanography Letters* 4: 155–163. https://doi.org/10.1002/lol2.10112.

Creed, I.F., S.E. Sanford, F.D. Beall, L.A. Molot, and P.J. Dillon. 2003. Cryptic wetlands: Integrating hidden wetlands in regression models of the export of dissolved organic carbon from forested landscapes. *Hydrological Processes* 17: 3629–3648.

Crosswell, J.R., M.S. Wetz, B. Hales, and H.W. Paerl. 2014. Extensive CO2 emissions from shallow coastal waters during passage of hurricane Irene (august 2011) over the mid-Atlantic Coast of the U.S.A. *Limnology and Oceanography* 59: 1651–1665.

Dickson, A.G., D.J. Wesolowski, D.A. Palmer, and R.E. Mesmer. 1990. Dissociation constant of bisulfate ion in aqueous sodium chloride solutions to 250.Degree.C. *The Journal of Physical Chemistry* 94: 7978–7985.

Duarte, C. 1991. Allometric scaling of seagrass form and productivity. Marine ecology progress series. *Marine Ecology Progress Series* 77: 289–300.

Emanuel, K. 2017. Assessing the present and future probability of Hurricane Harvey's rainfall. *Proceedings of the National Academy of Sciences* 114: 12681–12684.

Frid, C.L.J., and C.R. Townsend. 1989. An appraisal of the patch dynamics concept in stream and marine benthic communities whose members are highly mobile. *Oikos* 56: 137–141.

Galtsoff, P. 1964. The American oyster Crassostrea virginica Gmelin. *US Fisheries Bulletin* 64: 1–480.

Gotelli, N.J., and A.M. Ellison. 2013. *A primer of ecological statistics*. Sunderland: Sinauer Associates Inc.

Greening, H., P. Doering, and C. Corbett. 2006. Hurricane impacts on coastal ecosystems. *Estuaries and Coasts* 29: 877–879.

Gruber, R.K., D.C. Hinkle, and W.M. Kemp. 2011. Spatial patterns in water quality associated with submersed plant beds. *Estuaries and Coasts* 34: 961–972.

Guo, H., C. Weaver, S.P. Charles, A. Whitt, S. Dastidar, P. D'Odorico, J.D. Fuentes, J.S. Kominoski, A.R. Armitage, and S.C. Pennings. 2017. Coastal regime shifts: rapid responses of coastal wetlands to changes in mangrove cover. *Ecology* 98 (3): 762–772.

Harrison, G.W. 1979. Stability under environmental stress: resistance, resilience, persistence, and variability. *The American Naturalist* 113: 659–669.

Heck, K.L., G. Hays, and R.J. Orth. 2003. Critical evaluation of the nursery role hypothesis for seagrass meadows. *Marine Ecology Progress Series* 253: 123–136.

Hernandez-Delgado, E.A., C. Toledo-Hernandez, C.P. Diaz-Ruiz, N. Gomez-Andujar, J.L. Medina-Muniz, M.F. Canals-Silander, and S.E. Suleiman-Ramos. this volume. Hurricane impacts and the resilience of invasive and nuisance species on seagrasses: a case study from Puerto Rico. *Estuaries and Coasts*.

Hornberger, G.M., K.E. Bencala, and D.M. McKnight. 1994. Hydrological controls on dissolved organic carbon during snowmelt in the Snake River near Montezuma, Colorado. *Biogeochemistry* 25: 147–165.

Hosen, J.D., A.W. Armstrong, and M.A. Palmer. 2018. Dissolved organic matter variations in coastal plain wetland watersheds: the integrated role of hydrological connectivity, land use, and seasonality. *Hydrological Processes* 32: 1664–1681.

Hsu, S.A., E.A. Meindl, and D.B. Gilhousen. 1994. Determining the power-law wind-profile exponent under near-neutral stability conditions at sea. *Journal of Applied Meteorology* 33: 757–765.

Huisman, T.J., F. Van Langevelde, and W.F. De Boer. 2009. Local positive feedback and the persistence and recovery of fringe *Avicennia marina* (Forssk.) vierh. mangroves. *Wetlands Ecology and Management* 17: 601–611.

Ilg, C., F. Dziock, F. Foeckler, K. Follner, M. Gerisch, J. Glaeser, A. Rink, A. Schanowski, M. Scholz, O. Deichner, and K. Henle. 2008. Long-term reactions of plants and macroinvertebrates to extreme floods in floodplain grasslands. *Ecology* 89 (9): 2392–2398.

Imbert, D., A. Rousteau, and P. Scherrer. 2000. Ecology of mangrove growth and recovery in the lesser antilles: state of knowledge and basis for restoration projects. *Restoration Ecology* 8: 230–236.

IPCC. 2018. Global warming of 1.5°C. An IPCC Special Report on the impacts of global warming of 1.5°C above pre-industrial levels and related global greenhouse gas emission pathways. In *The context of strengthening the global response to the threat of climate change, sustainable development, and efforts to eradicate poverty*, ed. V. Masson-Delmotte, P. Zhai, H.O. Pörtner, D. Roberts, J. Skea, P.R. Shukla, A. Pirani, W. Moufouma-Okia, C. Péan, R. Pidcock, S. Connors, J.B.R. Matthews, Y. Chen, X. Zhou, M.I. Gomis, E. Lonnoy, T. Maycock, M. Tignor, and T. Waterfield. Geneva: World Meteorological Organization.

Jiang, L.-Q., W.-J. Cai, and Y. Wang. 2008. A comparative study of carbon dioxide degassing in river- and marine-dominated estuaries. *Limnology and Oceanography* 53: 2603–2615.

Kaldy, J.E., and K.H. Dunton. 2000. Above- and below-ground production, biomass and reproductive ecology of *Thalassia testudinum* (turtle grass) in a subtropical coastal lagoon. *Marine Ecology Progress Series* 193: 271–283.

Knutson, T.R., J.L. McBride, J. Chan, K. Emanuel, G. Holland, C. Landsea, I. Held, J.P. Kossin, A.K. Srivastava, and M. Sugi. 2010. Tropical cyclones and climate change. *Nature Geoscience* 3: 157.

Koenker, R. 2018. *quantreg: Quantile Regression*. R package version 5.35.

La Peyre, M.K., B. Gossman, and J.F. La Peyre. 2009. Defining optimal freshwater flow for oyster production: effects of freshet rate and magnitude of change and duration on eastern oysters and Perkinsus marinus infection. *Estuaries and Coasts* 32: 522–534.

Laurance, W.F., and T.J. Curran. 2008. Impacts of wind disturbance on fragmented tropical forests: a review and synthesis. *Austral Ecology* 33: 399–408.

Laws, E.A. 2013. Evaluation of in situ phytoplankton growth rates: a synthesis of data from varied approaches. *Annual Review of Marine Science* 5: 247–268.

Levin, L.A. 1984. Life history and dispersal patterns in a dense infaunal polychaete assemblage: community structure and response to disturbance. *Ecology* 65: 1185–1200.

Likens, G.E., F.H. Bormann, N.M. Johnson, D.W. Fisher, and R.S. Pierce. 1970. Effects of forest cutting and herbicide treatment on nutrient budgets in the Hubbard Brook watershed-ecosystem. *Ecological Monographs* 40: 23–47.

Lundquist, C.J., S.F. Thrush, G. Coco, and J.E. Hewitt. 2010. Interactions between disturbance and dispersal reduce persistence thresholds in a benthic community. *Marine Ecology Progress Series* 413: 217–228.

Lytle, D.A., T. Bogan Michael, and S. Finn Debra. 2008. Evolution of aquatic insect behaviours across a gradient of disturbance predictability. *Proceedings of the Royal Society B: Biological Sciences* 275: 453–462.

Mallin, M., M. Posey, G. Shank, M. McIlver, S. Ensign, and T. Alphin. 1999. Hurricane effects on water quality and benthos in the cape fear watershed: natural and anthropogenic impacts. *Ecological Applications* 9: 350–362.

Mann, M.E., and K.A. Emanuel. 2006. Atlantic hurricane trends linked to climate change. *Eos, Transactions American Geophysical Union* 87: 233–241.

Massie, J., B. Strickland, R. Santos, J.P. Hernandez, N. Viadero, H. Willoughy, M. Heithaus, and J. Rehage. this volume. Going downriver: hurricane driven movements of common snook in response to environmental cues in a subtropical coastal river. *Estuaries and Coasts*.

McGarvey, D.J., J.A. Falke, H.W. Li, and J.L. Li. 2017. Fish assemblages. In *Methods in stream ecology volume 1: ecosystem structure*, ed. F.R. Hauer and G.A. Lamberti, 321–354. London: Academic Press.

McMillan, S.K., H.F. Wilson, C.L. Tague, D.M. Hanes, S. Inamdar, D.L. Karwan, T. Loecke, J. Morrison, S.F. Murphy, and P. Vidon. 2018. Before the storm: antecedent conditions as regulators of hydrologic and biogeochemical response to extreme climate events. *Biogeochemistry*.

McTigue, N.D., P. Bucolo, Z. Liu, and K.H. Dunton. 2015. Pelagic-benthic coupling, food webs, and organic matter degradation in the Chukchi Sea: insights from sedimentary pigments and stable carbon isotopes. *Limnology and Oceanography* 60: 429–445.

Millero, F.J. 2010. Carbonate constants for estuarine waters. *Marine and Freshwater Research* 61: 139–142.

Montagna, P.A., and R.D. Kalke. 1992. The effect of freshwater inflow on meiofaunal and macrofaunal populations in the Guadalupe and Nueces estuaries, Texas. *Estuaries* 15: 266–285.

Montagna, P.A., and R.D. Kalke. 1995. Ecology of infaunal mollusca in South Texas estuaries. *American Malacological Bulletin* 24: 101–115.

Montagna, P.A., and J.L. Li. 2010. Effect of freshwater inflow on nutrient loading and macrobenthos secondary production in Texas lagoons. In *Coastal lagoons: critical habitats of environmental change*, ed. M.J. Kennish and H.W. Paerl, 513–539. Boca Raton: CRC Press, Taylor & Francis Group.

Moore, J.L., B.J. Puckett, and S.J. Schreiber. 2018. Restoration of eastern oyster populations with positive density dependence. *Ecological Applications* 28 (4): 897–909.

Munroe, D., A. Tabatabai, I. Burt, D. Bushek, E.N. Powell, and J. Wilkin. 2013. Oyster mortality in Delaware Bay: impacts and recovery from Hurricane Irene and Tropical Storm Lee. *Estuarine, Coastal and Shelf Science* 135: 209–219.

Nelson, D. M. (ed.). 1992. *Distribution and abundance of fishes and invertebrates in Gulf of Mexico estuaries, volume I: data summaries. Estuarine Living Marine Resources Report 10*. Rockville: NOAA/NOS Strategic Environmental Assessments Division.

NOAA. 2018. Commercial fisheries statistics: NOAA Office of Science and Technology. *Marine Fisheries Service*.

Nordlie, F.G. 2003. Fish communities of estuarine salt marshes of eastern North America, and comparisons with temperate estuaries of other continents. *Reviews in Fish Biology and Fisheries* 13: 281–325.

Noss, R.F., W.J. Platt, B.A. Sorrie, A.S. Weakley, D.B. Means, J. Costanza, and R.K. Peet. 2015. How global biodiversity hotspots may go unrecognized: lessons from the North American Coastal Plain. *Diversity and Distributions* 21: 236–244.

Oksanen, J., F. Guillaume Blanchet, R. Kindt, P. Legendre, P.R. Minchin, R.B. O'Hara, G.L. Simpson, P. Solymos, M.H.H. Stevens, and H.

Wagner. 2014. *Vegan: community ecology package*. Version 2.1–41. http://r-forge.r-project.org/projects/vegan.

Orth, R.J., and D.J. Wilcox. 2009. Assessment of the abundance of submersed aquatic vegetation (SAV) communities in the Chesapeake Bay and its use in SAV management. In *Remote sensing and geospatial technologies for coastal ecosystems assessment and management, lecture notes in geoinformation and cartography*, ed. Y. Xiaojun, 233–257.

Orth, R.J., W.C. Dennison, J.S. Lefcheck, C. Gurbisz, M. Hannam, J. Keisman, J.B. Landry, K.A. Moore, R.R. Murphy, C.J. Patrick, J. Testa, D.E. Weller, and D.J. Wilcox. 2017. Submersed aquatic vegetation in Chesapeake Bay: sentinel species in a changing world. *BioScience* 67: 698–712.

Paerl, H.W., J.D. Bales, L.W. Ausley, C.P. Buzzelli, L.B. Crowder, L.A. Eby, J.M. Fear, M. Go, B.L. Peierls, T.L. Richardson, and J.S. Ramus. 2001. Ecosystem impacts of three sequential hurricanes (Dennis, Floyd, and Irene) on the United States' largest lagoonal estuary, Pamlico Sound, NC. *Proceedings of the National Academy of Sciences* 98: 5655–5660.

Pimm, S.L. 1984. The complexity and stability of ecosystems. *Nature* 307: 321.

Pinckney, J.L., H.W. Paerl, and M.B. Harrington. 1999. Responses of the phytoplankton community growth rate to nutrient pulses in variable estuarine environments. *Journal of Phycology* 35: 1455–1463.

Pinheiro, J., D. Bates, S. DebRoy, D. Sarkar, and R Core Team. 2017. _nlme: linear and nonlinear mixed effects models. R package version 3.1–131.

Popovich, C.A., C.V. Spetter, J.E. Marcovecchio, and R.H. Freije. 2008. Dissolved nutrient availability during winter diatom bloom in a turbid and shallow estuary (Bahía Blanca, Argentina). *Journal of Coastal Research* 2008 (95–102): 108.

Pruitt, J.N., A.G. Little, S.J. Majumdar, T.W. Schoener, and D.W. Fisher. 2019. Call-to-action: a global consortium for tropical cyclone ecology. *Trends in Ecology & Evolution* 34 (7): 588–590.

R Core Team. 2016. *R: a language and environment for statistical computing*. Vienna: R Foundation for Statistical Computing ISBN 3-900051-07-0.

Raymond, P.A., J.E. Saiers, and W.V. Sobczak. 2016. Hydrological and biogeochemical controls on watershed dissolved organic matter transport: pulse-shunt concept. *Ecology* 97 (1): 5–16.

Reese, M.M., G.W. Stunz, and A.M. Bushon. 2008. Recruitment of estuarine-dependent nekton through a new tidal inlet: the opening of Packery Channel in Corpus Christi, TX, USA. *Estuaries and Coasts* 31: 1143–1157.

Reyna, N.E., A.K. Hardison, and Z. Liu. 2017. Influence of major storm events on the quantity and composition of particulate organic matter and the phytoplankton community in a subtropical estuary, Texas. *Frontiers in Marine Science* 4.

Richardson, M.C., C.P.J. Mitchell, B.A. Branfireun, and R.K. Kolka. 2010. Analysis of airborne LiDAR surveys to quantify the characteristic morphologies of northern forested wetlands. *Journal of Geophysical Research: Biogeosciences* 115.

Roth, L.C. 1992. Hurricanes and mangrove regeneration: effects of hurricane Joan, October 1988, on the vegetation of Isla del Venado, Bluefields, Nicaragua. *Biotropica* 24: 375–384.

Schaefer, D.A., W.H. McDowell, F.N. Scatena, and C.E. Asbury. 2000. Effects of hurricane disturbance on stream water concentrations and fluxes in eight tropical forest watersheds of the Luquillo experimental forest, Puerto Rico. *Journal of Tropical Ecology* 16: 189–207.

Seager, R., M. Ting, I. Held, Y. Kushnir, J. Lu, G. Vecchi, H.-P. Huang, N. Harnik, A. Leetmaa, N.-C. Lau, C. Li, J. Velez, and N. Naik. 2007. Model projections of an imminent transition to a more arid climate in southwestern North America. *Science* 316: 1181–1184.

Seager, R., M. Ting, C. Li, N. Naik, B. Cook, J. Nakamura, and H. Liu. 2013. Projections of declining surface-water availability for the southwestern United States. *Nature Climate Change* 3: 482–486.

Smith, I.I.I.T.J., M.B. Robblee, H.R. Wanless, and T.W. Doyle. 1994. Mangroves, hurricanes, and lightning strikes assessment of Hurricane Andrew suggests an interaction across two differing scales of disturbance. *BioScience* 44: 256–262.

Smith, T.J., G.H. Anderson, K. Balentine, G. Tiling, G.A. Ward, and K.R.T. Whelan. 2009. Cumulative impacts of hurricanes on Florida mangrove ecosystems: sediment deposition, storm surges and vegetation. *Wetlands* 29: 24.

Solis, R.S., and G.L. Powell. 1998. Hydrography, mixing characteristics, and residence times of Gulf of Mexico estuaries. In *Biogeochemistry of Texas estuaries*, ed. T.S. Bianchi, J.R. Pennock, and R.Y. Twilley, 29–61. Oxford: OxfordUniversity Press.

Sorrie, B.A., and A.S. Weakley. 2001. Coastal plain vascular plant endemics: phytogeographic patterns. *Castanea* 66: 50–82.

Sun, M., R. Aller, and C.Y. Lee. 1991. Early diagenesis of chlorophyll-a in Long Island Sound sediments - a measure of carbon flux and particle reworking. *Journal of Marine Research* 49: 379–401.

Tomlinson, P. 2016. *The botany of mangroves*. Cambridge: Cambridge University Press.

Townsend, C.R. 1989. The patch dynamics concept of stream community ecology. *Journal of the North American Benthological Society* 8: 36–50.

Uppstrom, L.R. 1974. The boron/chlorinity ratio of deep-sea water from the Pacific Ocean. *Deep Sea Research Part A. Oceanographic Research Papers*: 161-162.

USGS. 2016. *National Water Information System*. Data available on the World Wide Web (USGS Water Data for the Nation).

van der Heide, T., E.H. van Nes, M.M. van Katwijk, H. Olff, and A.J.P. Smolders. 2011. Positive feedbacks in seagrass ecosystems – evidence from large-scale empirical data. *PLoS One* 6: e16504.

VanDiggelen, A., and P.A. Montagna. 2016. Is salinity variability a benthic disturbance in estuaries? *Estuaries and Coasts* 39: 967–980.

Wachnicka, A., J. Browder, T. Jackson, W. Louda, C. Kelble, O. Abdelrahman, E. Stabenau, and C. Avila. 2019. Hurricane Irma's impact on water quality and phytoplankton communities of Biscayne Bay (Florida, USA). *Estuaries and Coasts*.

Watanabe, K., and T. Kuwae. 2015. How organic carbon derived from multiple sources contributes to carbon sequestration processes in a shallow coastal system? *Global Change Biology* 21 (7): 2612–2623.

Weiss, R.F. 1974. Carbon dioxide in water and seawater: the solubility of a non-ideal gas. *Marine Chemistry* 2: 203–215.

Weiss, R.F., and B.A. Price. 1980. Nitrous oxide solubility in water and seawater. *Marine Chemistry* 8: 347–359.

Whitfield, P.E., W.J. Kenworthy, M.J. Durako, K.K. Hammerstrom, and M.F. Merello. 2004. Recruitment of *Thalassia testudinum* seedlings into physically disturbed seagrass beds. *Marine Ecology Progress Series* 267: 121–131.

Xi, W. 2015. Synergistic effects of tropical cyclones on forest ecosystems: a global synthesis. *Journal of Forestry Research* 26: 1–21.

Yao, H., and X. Hu. 2017. Responses of carbonate system and CO2 flux to extended drought and intense flooding in a semiarid subtropical estuary. *Limnology and Oceanography* 62: S112–S130.

Yao, H., M.R. McCutcheon, C.J. Staryk, and X. Hu. 2020. Hydrologic controls on CO2 chemistry and flux in subtropical lagoonal estuaries of the northwestern Gulf of Mexico. *Limnology and Oceanography* in revision.

Zieman, J.C. 1976. The ecological effects of physical damage from motor boats on turtle grass beds in Southern Florida. *Aquatic Botany* 2: 127–139.

Zink, I., J. Browder, and C. Kelble. this volume. Extreme hurricane disturbance mediated shifts of a subtropical seagrass associated fish and macroinvertebrate community. *Estuaries and Coasts*.